

RISnet: A Domain-Knowledge Driven Neural Network Architecture for RIS Optimization with Mutual Coupling and Partial CSI

Bile Peng, *Senior Member, IEEE*, Karl-Ludwig Besser, *Member, IEEE*, Shanpu Shen, *Senior Member, IEEE*, Finn Siegismund-Poschmann, Ramprasad Raghunath, *Student Member, IEEE*, Daniel Mittleman, *Fellow, IEEE*, Vahid Jamali, *Senior Member, IEEE*, and Eduard A. Jorswieck, *Fellow, IEEE*

Abstract—Space-division multiple access (SDMA) plays an important role in modern wireless communications. Its performance depends on the channel properties, which can be improved by reconfigurable intelligent surfaces (RISs). In this work, we jointly optimize SDMA precoding at the base station (BS) and RIS configuration. We tackle difficulties of mutual coupling between RIS elements, scalability to more than 1000 RIS elements, and high requirement for channel estimation. We first derive an RIS-assisted channel model considering mutual coupling, then propose an unsupervised machine learning (ML) approach to optimize the RIS with a dedicated neural network (NN) architecture *RISnet*, which has good scalability, desired permutation-invariance, and a low requirement for channel estimation. Moreover, we leverage existing high-performance analytical precoding scheme to propose a hybrid solution of ML-enabled RIS configuration and analytical precoding at BS. More generally, this work is an early contribution to combine ML technique and domain knowledge in communication for NN architecture design. Compared to generic ML, the problem-specific ML can achieve higher performance, lower complexity and permutation-invariance.

Index Terms—Mutual coupling, Partial channel state information, Ray-tracing channel model, Reconfigurable intelligent surfaces, Space-division multiple access, Unsupervised machine learning.

Parts of this work were presented at the 2023 IEEE Global Communications Conference (GlobeCom) [1].

B. Peng, R. Raghunath and E. A. Jorswieck are with Institute for Communications Technology, TU Braunschweig, Germany (e-mail: {b.peng, r.raghunath, e.jorswieck}@tu-braunschweig.de). K.-L. Besser was with the Department of Electrical and Computer Engineering, Princeton University, Princeton, NJ 08544, USA, and is now with the Department of Electrical Engineering, Linköping University, Linköping, Sweden (email: karl-ludwig.besser@liu.se). S. Shen is with Department of Electrical Engineering and Electronics, University of Liverpool, UK (email: Shanpu.Shen@liverpool.ac.uk). F. Siegismund-Poschmann is with Institute for Computer Science, Freie Universität Berlin, Germany (email: finn.siegismund-poschmann@fu-berlin.de). V. Jamali is with the Department of Electrical Engineering and Information Technology, TU Darmstadt, Germany (email: vahid.jamali@tu-darmstadt.de). D. Mittleman is with School of Engineering, Brown University, USA (email: daniel_mittleman@brown.edu).

The work of E. Jorswieck, R. Raghunath, and B. Peng was supported partly by the Federal Ministry of Education and Research (BMBF), Germany, through the Program of Souverän, Digital, and Vernetzt Joint Project 6G-RIC under Grant 16KISK031. The work of K.-L. Besser was supported by the German Research Foundation (DFG) under grant BE 8098/1-1. The work of V. Jamali is supported in part by the DFG within the Collaborative Research Center MAKI (SFB 1053, Project-ID 210487104) and in part by the LOEWE initiative (Hesse, Germany) within the emergenCITY center [LOEWE/1/12/519/03/05.001(0016)/72]. The work of D. Mittleman is supported by the US National Science Foundation (CNS-1954780, CNS-2211616), the US Air Force Office of Scientific Research (FA9550-22-1-0412), the Alexander von Humboldt Foundation, and the DFG through a Mercator Fellowship.

I. INTRODUCTION

The space-division multiple access (SDMA) technique plays an important role in modern multi-user wireless communications. Its performance depends heavily on the channel condition. For example, a high channel gain realizes a high signal-to-noise ratio (SNR), a high-rank multiple-input-multiple-output (MIMO) channel matrix makes it possible to serve multiple users [2]. In the past, the wireless channel has been considered as given. However, in recent years, the reconfigurable intelligent surface (RIS) [3] has been proposed to manipulate the channel property. In this paper, we consider the problem of joint optimization of precoding at the base station (BS) and configuration of the RIS.

In the literature, multiple precoding techniques have been proposed for SDMA at the BS, including maximum ratio transmission (MRT), zero-forcing (ZF), minimum mean square error (MMSE) precoding [4], and weighted minimum mean square error (WMMSE) precoding with proved equivalence to weighted sum-rate (WSR) maximization [5]. The joint optimization of precoding and RIS configuration was performed with block coordinate descent (BCD) [6], majorization-minimization (MM) [7], [8] and alternating direction method of multipliers (ADMM) [9] algorithms to maximize the WSR in SDMA. In addition, Riemannian manifold conjugate gradient (RMCG) and Lagrangian method were applied to optimize multiple RISs and BSs to serve cell-edge users [10]. Successive refinement algorithm and exhaustive search were applied for passive beamforming improvement [11]. The active RISs was optimized with the successive convex approximation (SCA) algorithm to maximize the SNR [12]. The gradient-based optimization was applied to optimize the effective rank and the minimum singular value [13]. A novel alternating optimization (AO) scheme is proposed to minimize the transmit power subject to the data rate requirement [14]. A multi-layer refracting RIS is proposed for simultaneous wireless information and power transfer (SWIPT) to overcome severe large-scale fading [15].

In general, the above analytical iterative methods do not scale well with the number of RIS elements. No more than 100 elements were assumed in [6]–[12] and up to 400 RIS elements were assumed in [13], which is far from the vision of more than 1000 RIS elements [16] and the requirement in many scenarios to realize a necessary link budget [17]. Another common important limitation of the analytical optimization

approaches is that suboptimal approximations were applied to make the problem solvable [6], [9], [11]. Moreover, the required numbers of iterations make the proposed iterative algorithms difficult to be implemented in real time since the computation time is longer than the channel coherence time.

A noticeable effort is to apply machine learning (ML) to optimize the RIS, which bypasses the difficulty of analytical solution via the universal approximation property of the neural network (NN) [18]. Recently, deep learning (DL) and reinforcement learning (RL) were applied and compared for RIS optimization [19]. Long short-term memory (LSTM) and deep Q-network (DQN) were applied to optimize RIS for non-orthogonal multiple access (NOMA) [20]. RL was applied to maximize the sum-rate in SDMA [21], and NOMA [21], [22] and energy efficiency in NOMA [23]. The achievable rate was predicted and the RIS was configured with DL [24]. The RIS was configured directly with received pilot signals [25]. The mapping from received pilot signal to the phase shifts was optimized [26]. Due to the separation of training and testing phases, the trained ML model was able to be applied in real time. However, the scalability with the number of RIS elements was still limited [20]–[22], [25]–[27].

The second common limitation of many works on RIS is the full channel state information (CSI) assumption (e.g., [6], [8], [9], [11], [12]). Due to the large number of elements, the full CSI of all elements is very difficult to obtain in real time. Possible countermeasures are, e.g., codebook-based RIS optimization [17], [28]. However, the beam training is still a major limitation.

The third common limitation of many works is the assumption of perfect RIS without mutual coupling. Due to the small distance between two adjacent elements, there might exist certain mutual coupling in the RIS. In the literature, a single-input single-output (SISO) RIS-assisted system was optimized [29]. A mutual impedance-based communication model considering mutual coupling was presented [30]. A mutual coupling aware characterization and performance analysis of the RIS was introduced [31]. The RIS architecture was modeled and characterized using scattering parameter network analysis [32]. A closed-form expression of RIS-assisted MIMO channel model in a general sense, i.e., considering RIS mutual coupling, with the direct channel from BS to users and without the unilateral approximation [33], is still an open problem.

Summarizing the state-of-the-art, we identify three limitations of current RIS research: the insufficient consideration of mutual coupling, the poor scalability to consider more than 1000 RIS elements and the unrealistic assumption of full CSI.

In this work, we propose a dedicated NN architecture *RISnet* and an unsupervised ML approach to address these limitations. Our contribution is four-fold as follows.

- We derive an RIS channel model considering the mutual coupling between RIS elements. The derivation is based on the scattering parameter network analysis [32]. A closed-form expression is derived without unilateral approximation.
- We propose an NN architecture *RISnet* for RIS configuration. The number of *RISnet* parameters is independent of the number of RIS elements, enabling a high scalability

such that we can configure 1296 RIS elements within a few milliseconds. Compared to it, most conventional approaches in the literature assume no more than 100 RIS elements, as explained above. Furthermore, the *RISnet* is *permutation-invariant*, i.e., any permutation of users in the input has no impact on the RIS phase shifts because permutation of users has no impact on the SDMA problem.

- In addition to the scalability, the CSI is extremely difficult to obtain due to the large number of RIS elements. We propose an improved *RISnet*, where only a few RIS elements (in our paper, 16 out of 1296) are equipped with RF chains and can estimate the channel with the pilot signals from users. We demonstrate that *RISnet* can configure the phase shifts of all RIS elements with the partial CSI of a few RIS elements if the channel is sparse, which holds mostly in reality. In this way, a good compromise between hardware complexity and performance is achieved.
- We combine ML-enabled RIS configuration and analytical precoding. In this way, the performance of BS precoding is guaranteed because of the proven performance of analytical precodings, the difficulty of training is reduced because we do not need to optimize precoding.

We combine domain knowledge in communication and ML for NN architecture and training process design. It not only solves the RIS configuration problem, but can also inspire solutions to other problems. According to [34], incorporating domain knowledge is considered as one of the three grand challenges in ML. We show that an NN architecture tailored for the considered problem is superior in scalability, complexity, performance and robustness.

This work is based on our preliminary result [1]. Compared to it, we consider the mutual coupling between the RIS elements in this work. The mutual coupling is unavoidable due to the short distance between RIS elements. However, it has not been considered in most literature because the resulting optimization problem is too difficult. In addition, we maximize the WSR in this work instead of sum-rate in [1], where the weights are input of the *RISnet*. In this way, we significantly improve the flexibility to choose an operational point according to the requirement. Furthermore, we further propose a parallel implementation scheme with tensor operations, which allows for very efficient training and inference (application) in a GPU. The permutation-invariance is strictly proved. We also discuss possibilities to combine analytical precoding techniques with ML, depending on the differentiability of the analytical method.

Notations: $(\cdot)^+$ denotes the pseudo-inverse operation, $|a|$ and $\arg(a)$ are amplitude and phase of complex number a , respectively, $\mathbf{T}[:, j, k]$ denotes the vector of the elements with position (j, k) in the second and third dimensions in the three-dimensional tensor \mathbf{T} , $\mathbf{1}^{a \times a}$ is the matrix of all ones with shape $a \times a$, and $\mathbf{I}^{a \times a}$ is the identity matrix with shape $a \times a$, i.e., all diagonal elements of $\mathbf{I}^{a \times a}$ are ones, all off-diagonal elements are zeros. We also define $\mathbf{E}^{a \times a} = \mathbf{1}^{a \times a} - \mathbf{I}^{a \times a}$.

II. THE RIS CHANNEL MODEL CONSIDERING MUTUAL COUPLING

We consider a RIS-aided multi-user multiple-input-single-output (MISO) scenario, as depicted in Figure 1. The channel from BS to RIS is denoted as $\mathbf{H} \in \mathbb{C}^{N \times M}$, where N is the number of RIS elements and M is the number of BS antennas. The channel from RIS to users is denoted as $\mathbf{G} \in \mathbb{C}^{U \times N}$, where U is the number of users. The direct channel from BS to users directly is denoted as $\mathbf{D} \in \mathbb{C}^{U \times M}$.

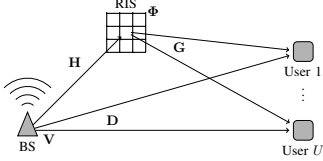


Figure 1. The system model of RIS-assisted downlink multi-user broadcasting.

Denote the precoding matrix as $\mathbf{V} \in \mathbb{C}^{M \times U}$ and the signal processing matrix of the RIS as the diagonal matrix $\Phi \in \mathbb{C}^{N \times N}$, where the diagonal element in row n and column n is $\phi_{nn} = e^{j\psi_n}$, with $\psi_n \in [0, 2\pi)$ being the phase shift of RIS element n . Conventionally, the channel \mathbf{C} between BS and users is [6]

$$\mathbf{C} = \mathbf{D} + \mathbf{G}\Phi\mathbf{H}, \quad (1)$$

and the signal received at the users is

$$\mathbf{y} = \mathbf{C}\mathbf{V}\mathbf{x} + \mathbf{n}, \quad (2)$$

where $\mathbf{x} \in \mathbb{C}^{U \times 1}$ is the transmitted symbols, $\mathbf{y} \in \mathbb{C}^{U \times 1}$ is the received symbols, and $\mathbf{n} \in \mathbb{C}^{U \times 1}$ is the noise.

An implicit assumption of (1) is that the RIS elements do not have mutual coupling. However, this assumption might not hold due to the small distance between RIS elements. In the following, we assume transmitter and receiver without mutual coupling and an RIS with mutual coupling.

Our derivation is a generalization of Section III in [32]. We define the S-parameter matrix \mathbf{S} for the signal transmission system shown in Figure 1 and partition it as

$$\mathbf{S} = \begin{bmatrix} \mathbf{S}_{TT} & \mathbf{S}_{TI} & \mathbf{S}_{TR} \\ \mathbf{S}_{IT} & \mathbf{S}_{II} & \mathbf{S}_{IR} \\ \mathbf{S}_{RT} & \mathbf{S}_{RI} & \mathbf{S}_{RR} \end{bmatrix}, \quad (3)$$

where index T stands for transmitter, I stands for RIS and R stands for receiver. The diagonal blocks \mathbf{S}_{TT} , \mathbf{S}_{II} and \mathbf{S}_{RR} are the S-matrices of transmitter, RIS and receiver, respectively. The off-diagonal blocks \mathbf{S}_{TI} , \mathbf{S}_{TR} and \mathbf{S}_{IR} are the channels between transmitter and RIS, transmitter and receivers, and RIS and receivers, respectively, i.e., the channels \mathbf{H} , \mathbf{D} and \mathbf{G} in Figure 1, respectively. We also have the diagonal reflection coefficient matrix Λ , which is defined as

$$\Lambda = \begin{bmatrix} \Lambda_T & \mathbf{0} & \mathbf{0} \\ \mathbf{0} & \Phi & \mathbf{0} \\ \mathbf{0} & \mathbf{0} & \Lambda_R \end{bmatrix}, \quad (4)$$

where Λ_T , Φ and Λ_R are the reflection coefficient matrices of transmitter, RIS and receiver, respectively. Define $\mathbf{T} = \mathbf{S}(\mathbf{I} - \Lambda\mathbf{S})^{-1}$ and partition \mathbf{T} as

$$\mathbf{T} = \begin{bmatrix} \mathbf{T}_{TT} & \mathbf{T}_{TI} & \mathbf{T}_{TR} \\ \mathbf{T}_{IT} & \mathbf{T}_{II} & \mathbf{T}_{IR} \\ \mathbf{T}_{RT} & \mathbf{T}_{RI} & \mathbf{T}_{RR} \end{bmatrix} \quad (5)$$

in the same way as (3). According to [32], the channel matrix is given by

$$\mathbf{C} = (\Lambda_R + \mathbf{I})\mathbf{T}_{RT}(\mathbf{I} + \Lambda_T\mathbf{T}_{TT} + \mathbf{T}_{TT})^{-1}. \quad (6)$$

Although (6) is the most general form of the channel, it is too complicated for the optimization due to the matrix multiplication and inversion. In the following, we simplify (6) assuming no mutual coupling at transmitter and receiver, i.e., $\mathbf{S}_{TT} = \mathbf{0}$ and $\mathbf{S}_{RR} = \mathbf{0}$, and mutual coupling at RIS, i.e., $\mathbf{S}_{II} \neq \mathbf{0}$, the S-parameter matrix is

$$\mathbf{S} = \begin{bmatrix} \mathbf{0} & \mathbf{S}_{TI} & \mathbf{S}_{TR} \\ \mathbf{S}_{IT} & \mathbf{S}_{II} & \mathbf{S}_{IR} \\ \mathbf{S}_{RT} & \mathbf{S}_{RI} & \mathbf{0} \end{bmatrix}. \quad (7)$$

We further assume transmitter and receiver with perfect impedance matching, i.e., $\Lambda_T = \mathbf{0}$ and $\Lambda_R = \mathbf{0}$, we have

$$\Lambda = \begin{bmatrix} \mathbf{0} & \mathbf{0} & \mathbf{0} \\ \mathbf{0} & \Phi & \mathbf{0} \\ \mathbf{0} & \mathbf{0} & \mathbf{0} \end{bmatrix}. \quad (8)$$

Combining (7) and (8), we have

$$\Lambda\mathbf{S} = \begin{bmatrix} \mathbf{0} & \mathbf{0} & \mathbf{0} \\ \Phi\mathbf{S}_{IT} & \Phi\mathbf{S}_{II} & \Phi\mathbf{S}_{IR} \\ \mathbf{0} & \mathbf{0} & \mathbf{0} \end{bmatrix}. \quad (9)$$

Applying the Neumann series, we have

$$(\mathbf{I} - \Lambda\mathbf{S})^{-1} = \sum_{k=0}^{\infty} (\Lambda\mathbf{S})^k. \quad (10)$$

Combining (9) and (10), we obtain the first line of (11) at the top of the next page. Applying the Neumann series again in the opposite direction, we obtain the second line of (11). Combine (7), (5), and (11), we have

$$\mathbf{T}_{TT} = \mathbf{S}_{TI}(\mathbf{I} - \Phi\mathbf{S}_{II})^{-1}\Phi\mathbf{S}_{IT} \quad (12)$$

and

$$\mathbf{T}_{RT} = \mathbf{S}_{RT} + \mathbf{S}_{RI}(\mathbf{I} - \Phi\mathbf{S}_{II})^{-1}\Phi\mathbf{S}_{IT}. \quad (13)$$

According to (6), the channel matrix is

$$\mathbf{C} = (\mathbf{S}_{RT} + \mathbf{S}_{RI}(\mathbf{I} - \Phi\mathbf{S}_{II})^{-1}\Phi\mathbf{S}_{IT}) \cdot (\mathbf{I} + \mathbf{S}_{TI}(\mathbf{I} - \Phi\mathbf{S}_{II})^{-1}\Phi\mathbf{S}_{IT})^{-1} \quad (14)$$

where the term $\mathbf{S}_{TI}(\mathbf{I} - \Phi\mathbf{S}_{II})^{-1}\Phi\mathbf{S}_{IT}$ stands for the second order reflection from transmitter to RIS and back to transmitter,

$$\begin{aligned}
(\mathbf{I} - \mathbf{A}\mathbf{S})^{-1} &= \sum_{k=0}^{\infty} (\mathbf{A}\mathbf{S})^k = \begin{bmatrix} \mathbf{I} & \mathbf{0} & \mathbf{0} \\ \sum_{k=1}^{\infty} ((\mathbf{\Phi}\mathbf{S}_{II})^{k-1}) \mathbf{\Phi}\mathbf{S}_{IT} & \sum_{k=0}^{\infty} (\mathbf{\Phi}\mathbf{S}_{II})^k & \sum_{k=1}^{\infty} ((\mathbf{\Phi}\mathbf{S}_{II})^{k-1}) \mathbf{\Phi}\mathbf{S}_{IR} \\ \mathbf{0} & \mathbf{0} & \mathbf{I} \end{bmatrix} \\
&= \begin{bmatrix} \mathbf{I} & \mathbf{0} & \mathbf{0} \\ (\mathbf{I} - \mathbf{\Phi}\mathbf{S}_{II})^{-1} \mathbf{\Phi}\mathbf{S}_{IT} & (\mathbf{I} - \mathbf{\Phi}\mathbf{S}_{II})^{-1} & (\mathbf{I} - \mathbf{\Phi}\mathbf{S}_{II})^{-1} \mathbf{\Phi}\mathbf{S}_{IR} \\ \mathbf{0} & \mathbf{0} & \mathbf{I} \end{bmatrix}
\end{aligned} \tag{11}$$

which is negligible compared to \mathbf{I} in most communication systems¹. If we ignore this term, we have

$$\mathbf{C} = \mathbf{S}_{RT} + \mathbf{S}_{RI}(\mathbf{I} - \mathbf{\Phi}\mathbf{S}_{II})^{-1} \mathbf{\Phi}\mathbf{S}_{IT}. \tag{15}$$

Replacing \mathbf{S}_{IT} , \mathbf{S}_{RT} and \mathbf{S}_{RI} with more conventional \mathbf{H} , \mathbf{D} and \mathbf{G} , respectively, in the channel model context, we have

$$\mathbf{C} = \mathbf{D} + \mathbf{G}(\mathbf{I} - \mathbf{\Phi}\mathbf{S}_{II})^{-1} \mathbf{\Phi}\mathbf{H}. \tag{16}$$

In particular, if the RIS does not have mutual coupling, we have $\mathbf{S}_{II} = \mathbf{0}$ and (16) is reduced to (1). In this work, we apply the model from [30] to obtain the \mathbf{S}_{II} matrix.

Remark 1. Our channel model (16) is the same as the channel model (80) in [33]. However, the derivation in [33] requires the unilateral assumption, i.e., the channel from receiver to transmitter is ignored, which contradicts the channel reciprocity, i.e., channel gain from transmitter to receiver is equal to channel gain from receiver to transmitter. The reciprocity is an essential property of wireless channels. We obtain the same channel model without the unilateral assumption, making our derivation scientifically more rigorous.

Remark 2. The matrix inverse in (16) has a prohibitively high complexity. Therefore, we define $\mathbf{X} = \mathbf{G}(\mathbf{I} - \mathbf{\Phi}\mathbf{S}_{II})^{-1}$ and obtain \mathbf{X} by solving the linear equation system $\mathbf{X}(\mathbf{I} - \mathbf{\Phi}\mathbf{S}_{II}) = \mathbf{G}$. The differentiable LU decomposition is applied to solve the equation system, which has a significantly lower computation complexity. The channel model (16) becomes $\mathbf{C} = \mathbf{D} + \mathbf{X}\mathbf{\Phi}\mathbf{H}$.

III. PROBLEM FORMULATION

With the derived channel model from Section II, we can formulate the communication system optimization problems with SDMA, which uses the same resource block to serve multiple users. Therefore, it realizes a higher spectrum efficiency compared to earlier multiple access (MA) techniques, such as time domain multiple access (TDMA), frequency domain multiple access (FDMA) and code domain multiple access (CDMA) [35]. Moreover, SDMA gains popularity due to the high spatial resolution of modern massive multi-antenna systems [4]. Therefore, we choose SDMA a high-performance and future-oriented MA technique. In SDMA, the interference

from other users is considered as noise and the objective is to maximize the signal-to-interference-plus-noise ratio (SINR). we define $\mathbf{L} = \mathbf{C}\mathbf{V}$ with $\mathbf{L} \in \mathbb{C}^{U \times U}$. The SINR of user u is computed as $|l_{uu}|^2 / (\sum_{v \neq u} |l_{uv}|^2 + \sigma^2)$, where l_{uv} is the element in row u and column v of \mathbf{L} and σ^2 is the noise power. Following the canonical problem formulation of SDMA [5], we aim to maximize the WSR of all users. The problem is formulated as

$$\max_{\mathbf{V}, \mathbf{\Phi}} f = \sum_{u=1}^U w_u \log_2 \left(1 + \frac{|l_{uu}|^2}{\sum_{v \neq u} |l_{uv}|^2 + \sigma^2} \right) \tag{17a}$$

$$\text{s.t. } \text{Tr}(\mathbf{V}\mathbf{V}^H) \leq E_{Tr}, \tag{17b}$$

$$|\phi_{nn}| = 1 \text{ for } n = 1, \dots, N, \tag{17c}$$

$$|\phi_{nn'}| = 0 \text{ for } n, n' = 1, \dots, N \text{ and } n \neq n', \tag{17d}$$

where w_u in (17a) is the weight of user u , (17b) states that the total transmit power cannot exceed the maximum transmit power E_{Tr} , ϕ_{nn} in (17c) is the diagonal element in row n and column n of $\mathbf{\Phi}$. This constraint ensures that the RIS does not amplify the received signal (i.e., passive RIS). Constraint (17d) enforces that $\mathbf{\Phi}$ is diagonal. Note that l_{uv} depends on both \mathbf{V} and $\mathbf{\Phi}$. Therefore, both \mathbf{V} and $\mathbf{\Phi}$ are the optimization variables.

Remark 3. The maximal number of served users is the rank of channel \mathbf{C} . If the direct channel \mathbf{D} is weak, the rank of \mathbf{C} depends mainly on the rank of $\mathbf{G}(\mathbf{I} - \mathbf{\Phi}\mathbf{S}_{II})^{-1} \mathbf{\Phi}\mathbf{H}$. Since the rank of the product of matrices is smaller than or equal to the lowest rank of the factors, the rank of \mathbf{C} depends strongly on ranks of \mathbf{G} and \mathbf{H} . If they are rank-deficient, it is impossible to serve as many users as the BS antenna numbers.

In the following sections, we propose the unsupervised ML approach to solve Problem (17).

Remark 4. In Section IV, two approaches with full CSI and partial CSI are proposed. They share the same problem formulation (17). The only difference is the available information: With full CSI as the algorithm input, the objective (17a) can be computed in a deterministic way and the problem is easier to solve. However, the full CSI is difficult to obtain. With partial CSI, the information is incomplete to calculate the objective, because the CSI computation requires the full CSI, and the problem is more difficult to solve. However, the partial CSI is easier to obtain given limited resource for channel estimation, as will be explained in more detail in Section IV-C2.

IV. UNSUPERVISED MACHINE LEARNING WITH RISNET

A. The Framework of Unsupervised ML for Optimization

We first present the framework of unsupervised ML for optimization. Given a problem representation $\mathbf{\Gamma}$ (in our case,

¹According to the physics of electromagnetic wave propagation, i.e., the Friis transmission equation, only a small portion of the transmitted energy reaches the receiver due to the significant free-space path loss over distance. For instance, at a frequency of 3.5 GHz and a propagation distance of 20 m, the channel gain is approximately $(\lambda/(4\pi d))^2 = 1.2 \times 10^{-7}$, where λ is the wavelength and d is the propagation distance. The square of this gain, representing second-order reflections or higher-order effects, is approximately 1.44×10^{-14} , diminishing to negligible levels. Consequently, the term $\mathbf{S}_{TI}(\mathbf{I} - \mathbf{\Phi}\mathbf{S}_{II})^{-1} \mathbf{\Phi}\mathbf{S}_{IT}$ is orders of magnitude smaller than \mathbf{I} and can be ignored.

CSI and user weights w_u in (17a)), we look for a solution Φ (the RIS phase shifts) that maximizes objective f in (17a), which is fully determined by Γ and Φ , and it can be written as $f(\Gamma, \Phi)$. We define an NN N_θ , which is parameterized by θ (i.e., θ contains all trainable weights and biases in N_θ) and maps from Γ to Φ , i.e., $\Phi = N_\theta(\Gamma)$. We write the objective as $f(\Gamma, \Phi) = f(\Gamma, N_\theta(\Gamma); \theta)$. Note that it is emphasized that f depends on θ . We then collect massive data of Γ in a training set \mathcal{D} and formulate the problem as

$$\max_{\theta} K = \sum_{\Gamma \in \mathcal{D}} f(\Gamma, N_\theta(\Gamma); \theta). \quad (18)$$

In this way, N_θ is optimized for the ensemble of $\Gamma \in \mathcal{D}$ (*training*) using gradient ascent:

$$\theta \leftarrow \theta + \eta \nabla_{\theta} K, \quad (19)$$

where η is the learning rate. If N_θ is well trained, $\Phi' = N_\theta(\Gamma')$ is also a good solution for $\Gamma' \notin \mathcal{D}$ (*testing*), like a human uses experience to solve new problems of the same type² [36].

Although (18) is a general approach, it would benefit from the problem-specific domain knowledge. In the following sections, we first define the features. Next, we propose the RISnet architecture, and finally, we present the joint optimization of BS precoding and RIS configuration.

B. Channel Estimation and Feature Definition

To begin with the ML approach, we first define the features as input of RISnet. As depicted in Figure 1, there are three channel matrices \mathbf{H} , \mathbf{G} and \mathbf{D} , among which \mathbf{H} is assumed to be constant because BS and RIS are stationary and the environment is relatively invariant, \mathbf{G} and \mathbf{D} depend on the user positions. Therefore, they need to be estimated and used as input of N_θ . To estimate channel matrix \mathbf{G} , user u transmits a pilot signal ρ_u , which is known to the RIS. The received pilot signal is $v_{un} = g_{un}\rho + t$, where g_{un} is the channel gain between user u and RIS element n , and t is the thermal noise. The estimated value of g_{un} is therefore v_{un}/ρ_u . Note that we first assume that every RIS element has the ability to estimate the channels in Section IV-C1. This assumption is good for the optimization but requires expensive hardware. In Section IV-C2, we assume that only a few RIS elements are equipped with hardware for channel estimation with the pilot signals from users, which requires significantly less complicated hardware, but sets a more difficult challenge for the optimization. The estimation of the channel matrix \mathbf{D} is less challenging since the BS antennas are significantly less than the RIS elements. We can use a channel estimation method described in [6] to estimate \mathbf{D} . With the estimated channel matrices, we would like to define a feature γ_{un} for user u and RIS element n . Since g_{un} in row u and column n of \mathbf{G} is the channel gain from RIS element n to user u , we can simply include amplitude and phase of g_{un} in γ_{un} ³. On the other hand, elements in \mathbf{D} cannot be mapped to RIS elements because \mathbf{D} is the channel from the BS directly to the users. Therefore, we define $\mathbf{J} = \mathbf{D}\mathbf{H}^+$, and

(16) becomes $\mathbf{y} = (\mathbf{G}(\mathbf{I} - \Phi\mathbf{S}_{II})^{-1}\Phi + \mathbf{J})\mathbf{H}\mathbf{V}\mathbf{x} + \mathbf{n}$, i.e., signal \mathbf{x} is precoded with \mathbf{V} , transmitted through channel \mathbf{H} to the RIS, and through channel $\mathbf{G}(\mathbf{I} - \Phi\mathbf{S}_{II})^{-1}\Phi + \mathbf{J}$ to the users. Element j_{un} of \mathbf{J} can be interpreted as the channel gain from RIS element n to user u . The channel feature of user u and RIS element n can then be defined as $\gamma_{un} = (|g_{un}|, \arg(g_{un}), |j_{un}|, \arg(j_{un}))^T \in \mathbb{R}^{4 \times 1}$. The complete feature of all RIS elements and users is the aggregation of γ_{un} for all u and n and user weights. The concrete structure is described in the following Section IV-C.

C. The RISnet Architecture

We design a specific NN architecture for RIS configuration according to our domain knowledge in wireless communication. Observing (16), we notice that the optimal phase shift of every RIS element depends on its own channel gain and a common goal of the whole RIS, which should be shared among all RIS elements to enable their cooperation. Correspondingly, we define a *local feature* of every RIS element and a common *global feature* of all RIS elements. The RISnet consists of L layers. In each layer, we design information processing units to generate local features and global features for every RIS element and user, which are stacked as the input of the next layer, such that a proper information flow can be created for a sophisticated decision on Φ . The idea is comparable to using convolutional layers to capture local pattern in computer vision and using attention mechanism to model context in nature language processing, but for a much more specific problem with many RIS elements serving multiple users together.

By using the same information processing units for all RIS elements, the number of trainable parameters is independent of the number of RIS elements. With this approach, RISnet can configure more than 1000 elements with an adequate complexity, allowing for low complexity in training and high efficiency in inference (application).

Another important consideration from domain knowledge in communication is the *permutation-invariance*. From (17a), we notice that a permutation of the users does not have an impact on the objective function in SDMA. The optimal decision on Φ should therefore be independent from the user order. This property is called permutation-invariance. We define a permutation matrix $\mathbf{P} \in \{0, 1\}^{U \times U}$ to describe an arbitrary permutation, where each row and each column has only one 1. For example, let us define

$$\mathbf{P} = \begin{pmatrix} 1 & 0 & 0 \\ 0 & 0 & 1 \\ 0 & 1 & 0 \end{pmatrix}.$$

$\mathbf{P}\mathbf{G}$ permutes the second and third row of \mathbf{G} while the first row remains unchanged.

Definition 1. A neural network N_θ is permutation-invariant if $N_\theta(\mathbf{P}\Gamma) = N_\theta(\Gamma)$ for any permutation matrix \mathbf{P} .

It is desirable that RISnet is permutation-invariant for (17) to reflect the nature of SDMA.

A third consideration for RISnet design is that even if RISnet has a good scalability for more than one thousand RIS elements,

²A complete retraining is only required when the input states are fundamentally changed, e.g., change of deployment environment.

³The NN does not take complex numbers as input.

the full CSI of all RIS elements is extremely difficult to acquire. Therefore, it is very beneficial to have an input, which is easier to acquire than the full CSI.

1) *RISnet Architecture with Full CSI*: In the following, we present the RISnet architecture with the above-described high scalability with respect to (w.r.t.) RIS elements, permutation-invariance and low requirement for CSI input. The RISnet has multiple layers. Both input and output of a layer are three-dimensional tensors, where the first dimension is the feature, the second dimension is the RIS element and the third dimension is the user. In the first layer, the vector $\mathbf{f}_{un,1} = \mathbf{\Gamma}[\cdot, n, u]$ is the feature of RIS element n and user u , defined as the concatenation of user weight w_u and channel feature γ_{un} (defined in Section IV-B). The input and output feature format is shown in Figure 2.

As described at the beginning of this section, the decision on the optimal phase shift of every RIS element depends on both the local feature of the current RIS element and the global feature of the whole RIS. Therefore, for each RIS element and user, we define 4 classes of information processing units:

- current user and current RIS element (cc),
- current user and all RIS elements (ca),
- other users and current RIS element (oc),
- other users and all RIS elements (oa).

Denote the input feature of user u and RIS element n in layer i as $\mathbf{f}_{un,i}$, the output feature of user u and RIS element n in layer i is calculated as

$$\mathbf{f}_{un,i+1} = \begin{pmatrix} \text{ReLU}(\mathbf{W}_i^{\text{cc}} \mathbf{f}_{un,i} + \mathbf{b}_i^{\text{cc}}) \\ (\sum_{n'} \text{ReLU}(\mathbf{W}_i^{\text{ca}} \mathbf{f}_{un',i} + \mathbf{b}_i^{\text{ca}})) / N \\ \left(\sum_{u' \neq u} \text{ReLU}(\mathbf{W}_i^{\text{oc}} \mathbf{f}_{u'n,i} + \mathbf{b}_i^{\text{oc}}) \right) / (U - 1) \\ \left(\sum_{u' \neq u} \sum_{n'} \text{ReLU}(\mathbf{W}_i^{\text{oa}} \mathbf{f}_{u'n',i} + \mathbf{b}_i^{\text{oa}}) \right) / (N(U - 1)) \end{pmatrix} \quad (20)$$

for $i < L$, where $\mathbf{W}_i^{\text{cc}} \in \mathbb{R}^{Q_i \times P_i}$ is a matrix with trainable weights of class cc in layer i with the input feature dimension P_i in layer i (i.e., $\mathbf{f}_{un,i} \in \mathbb{R}^{P_i \times 1}$) and output feature dimension Q_i in layer i of class cc, $\mathbf{b}_i^{\text{cc}} \in \mathbb{R}^{Q_i \times 1}$ is trainable bias of class cc in layer i . Similar definitions and same dimensions apply to classes ca, oc and oa.

For class cc in layer i (the first line of (20)), the output feature of user u and RIS element n is computed by applying a conventional fully connected layer (a linear transform with weights \mathbf{W}_i^{cc} and bias \mathbf{b}_i^{cc} and the ReLU activation) to input $\mathbf{f}_{un,i}$. The difference to the conventional fully connected NN is that the information processing is applied to feature of every RIS element and user individually, instead of the whole input of all RIS elements and users.

For class ca in layer i (the second line of (20)), we first apply the conventional linear transform and ReLU activation to $\mathbf{f}_{un',i}$ like class cc, where $n = 1, \dots, N$, then compute the mean value of all RIS elements. Therefore, the output feature of class ca for user u and all RIS elements is the same.

For classes oc and oa (the third and fourth lines of (20)), the output features are averaged over all elements and/or other users, similar to class ca.

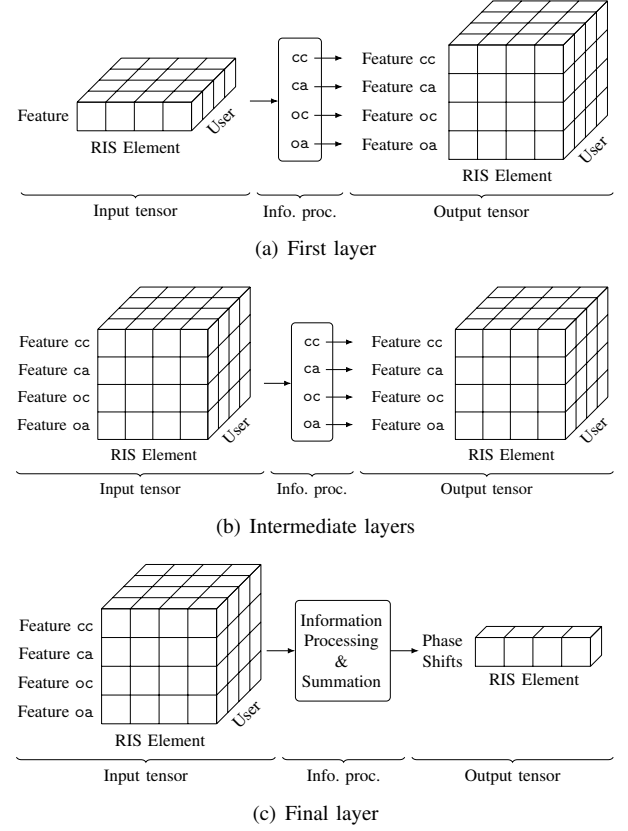


Figure 2. Information processing (info. proc.) in RISnet. The symmetric information processing along the dimension of users makes RISnet invariant to user permutation.

We can infer from the above description that $\mathbf{f}_{un,i+1} \in \mathbb{R}^{4Q_i}$ for all u and n because the output feature comprises of four classes. Therefore $P_{i+1} = 4Q_i$. The whole output feature $\mathbf{F}_{i+1} \in \mathbb{R}^{4Q_i \times U \times N}$ is a three dimensional tensor, where elements with index u and n in second and third dimensions are $\mathbf{f}_{un,i+1}$. Observe (20), we note that the same information processing units are applied to all users and RIS elements. Therefore, the number of trainable parameters is independent from the number of RIS elements, which enables a high scalability to configure more than 1000 RIS elements. For the final layer, we use one information processing unit. Features of different users are summed up to be the phase shifts because all the users share the same phase shift. Element ϕ_{nn} in row n and column n of Φ is defined as $\phi_{nn} = e^{j\varphi_n}$, where φ_n is the n -th output of RISnet. Since $|e^{j\varphi}| = 1$ for any φ , constraint (17c) is satisfied. Since all off-diagonal elements of Φ are initialized as 0 and stay constant during the optimization, constraint (17d) is satisfied. The information processing of a layer is illustrated in Figure 2.

Another important merit of RISnet for SDMA is the permutation-invariance.

Theorem 1. *The RISnet is permutation-invariant.*

Proof. The permutation-invariance can be intuitively achieved in the following way: Feature cc and Feature ca (current user and current/all RIS element(s)) depend only on the input feature of current user and are independent from user order. Feature

oc and Feature oa (other users and current/all RIS element(s)) depend only on the input feature of other users and are also independent from user order. Since the summation of features over all users in the last layer of RISnet is permutation-invariant, the RISnet is permutation-invariant. A rigid proof is available in Appendix A. \square

Remark 5. RISnet can be considered as a highly specialized graph neural network (GNN), which performs inference on a graph with vertices and edges between vertices. In our case, a vertex is a combination of RIS element and user. The class cc is the local feature of the vertex. Three sets of edges represent classes ca, oc and oa, where edges connect all RIS elements of the same user, users of the same RIS element, and all RIS elements and users, respectively. The messages passed from neighboring vertices in classes ca, oc and oa are described by lines two, three and four of (20), respectively. The aggregation of messages from neighboring vertices is the averaging operations in (20). The local feature and the global features are combined in the feature dimension as the input for the next layer.

2) *RISnet Architecture with Partial CSI:* Although the above-presented architecture has a high scalability due to the reuse of information processing units for all RIS elements and users, the channel estimation is still difficult. In particular, the estimation of \mathbf{G} is especially challenging due to the large number of RIS elements (unlike \mathbf{D}) and high variance since it depends on the user location (unlike \mathbf{H}). If every RIS element has the ability to estimate CSI from the pilot signal, the hardware would be very complex. However, using the domain knowledge in channel modeling, we notice that if the propagation paths in the channel are mostly line-of-sight (LoS) or specular, i.e., the channel is “sparse”, then the CSI of a few RIS elements contains sufficient information about the user location, which can be used to infer the full CSI of all RIS elements. This fact suggests that we can use *partial CSI* of \mathbf{G} as input to RISnet. The partial CSI is defined as channel gains between RIS and user of a few selected RIS elements equipped with hardware for channel estimation, i.e., a few selected columns of \mathbf{G} . The partial CSI can be estimated with received pilot signals from users. Since only a few RIS elements have hardware for channel estimation, the whole RIS has a low hardware complexity. Instead of performing an explicit full CSI prediction like an image super-resolution, we perform an implicit full CSI prediction, i.e., an end-to-end learning from partial CSI to a complete RIS configuration. In this section, we propose an RIS architecture where only a few RIS elements are equipped with hardware to estimate the CSI with pilot signals from the users, as described in Section IV-B. Compared to an RIS which can estimate full CSI, the proposed hardware architecture has a significantly lower complexity due to the small number of RIS elements with channel estimation ability. This hardware structure is similar to hybrid RIS [37], in which a few active elements with RF chains can amplify signals, but is simpler for implementation because the elements only estimate the channel rather than amplifying the signal, which justifies the feasibility of the proposed hardware architecture.

RIS elements with the hardware of channel estimation from received pilot signals of users are defined as *anchor elements*. They are uniformly placed on the RIS, because we would like to make the partial CSI as representative to the full CSI as possible. The geometric consideration will become clear in the following description.

The input channel features in this section consist of features of all users and anchor elements. The RISnet expands from the anchor elements to all RIS elements. A layer in RISnet that expands from anchor elements is called an *expansion layer*. The basic idea of the expansion layer is to apply the same information processing unit to an adjacent RIS element with the same relative position to the anchor element, as shown in Figure 3, where element 5 is an anchor element. The expansion layer computes features of all 9 elements with only feature of element 5 (\mathbf{f}_5). Therefore, each class, i.e., cc, ca, oc, oa for SDMA and c, a for NOMA, has 9 information processing units, which outputs features of the same RIS element and the adjacent 8 elements.

Concretely, the output of RIS element n using information processing unit j is computed as

$$\mathbf{f}_{uv(n,j),i+1} = \begin{pmatrix} \text{ReLU}(\mathbf{W}_{i,j}^{\text{cc}} \mathbf{f}_{un,i} + \mathbf{b}_{i,j}^{\text{cc}}) \\ (\sum_{n'} \text{ReLU}(\mathbf{W}_{i,j}^{\text{ca}} \mathbf{f}_{un',i} + \mathbf{b}_{i,j}^{\text{ca}})) / N \\ (\sum_{u' \neq u} \text{ReLU}(\mathbf{W}_{i,j}^{\text{oc}} \mathbf{f}_{u'n,i} + \mathbf{b}_{i,j}^{\text{oc}})) / (U - 1) \\ (\sum_{u' \neq u} \sum_{n'} \text{ReLU}(\mathbf{W}_{i,j}^{\text{oa}} \mathbf{f}_{u'n',i} + \mathbf{b}_{i,j}^{\text{oa}})) / (N(U - 1)) \end{pmatrix}, \quad (21)$$

where $\nu(n, j)$ is the RIS element index when applying information processing unit j for input of RIS element n . According to Figure 3 and assuming that the RIS element index begins with 1 at the upper left corner, increases first along the row and then changes to the next row (i.e., the index in row w and column h is $h + (w - 1) \cdot H$, with H being the number of columns of the RIS array), we have

$$\nu(n, j) = \begin{cases} n - H - 2 + j & j = 1, 2, 3, \\ n - 5 + j & j = 4, 5, 6, \\ n + H - 8 + j & j = 7, 8, 9. \end{cases} \quad (22)$$

In (21), we use the four information processing units defined in (20) to process feature of RIS element n and user u . Unlike in (20), where the output is feature of RIS element n and user u , the output in (21) is feature of RIS element $\nu(n, j)$ and user u . For example, for $j = 2$, the output feature is for the element above element n (see (22)). In this way, we generate features of 9 RIS elements out of the feature of 1 element.

By defining two such expansion layers, the numbers of anchor elements are increased by a factor of 9 in both row and column. If we have 16 anchor elements (4×4) with CSI, we can generate phase shifts of 1296 (36×36) RIS elements. The process of expanding anchor elements is illustrated in Figure 4, where the blue RIS elements in Figure 4(a) can estimate the channel from the pilot signals from the users. Such RIS elements are only 1/81 of all RIS elements. The whole RISnet architecture is shown in Figure 5.

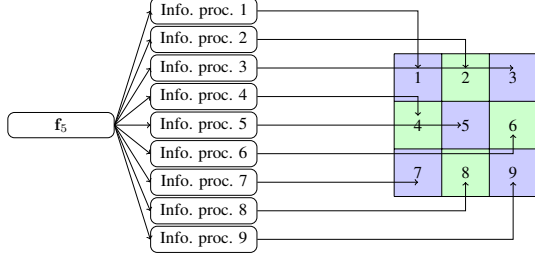


Figure 3. Application of 9 information processing units to expand from one anchor RIS element to 9 RIS elements, where f_5 is the channel feature of RIS element 5. Information processing unit 5 is comparable to the information processing units of RISnet with full CSI. Indices of user and layer are omitted for simplicity since the expansion is for RIS elements.

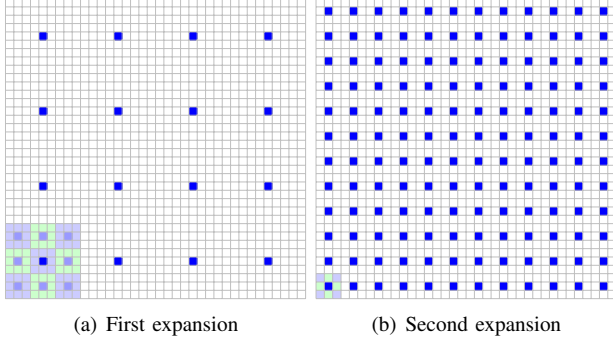


Figure 4. Expansion of considered RIS elements. Blue: anchor RIS elements. Lower left corner: example of the expansion to extend the anchor RIS elements from the blue element to the adjacent elements (light blue elements in Subfigure (a) and all elements in Subfigure (b)).

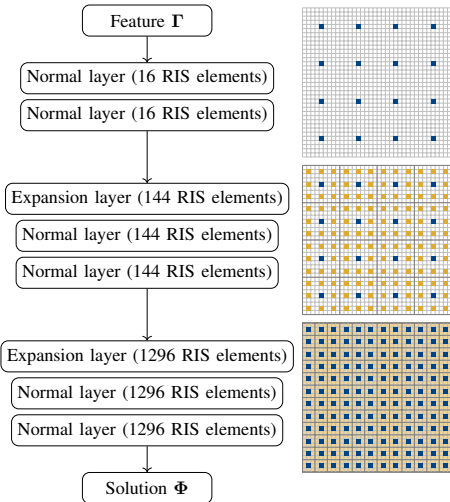


Figure 5. The RISnet architecture with partial CSI, where the information processing of normal layers is given by (20) and the information processing of expansion layers is given by (21). Note that this process is only possible with uniformly placed anchor elements.

Remark 6. The RIS elements with the channel estimation capability are fixed once the RIS hardware is designed. Since the hardware design does not change constantly, we assume known and fixed RIS elements with CSI. If the RIS layout is modified, the NN architecture must be modified accordingly. For example, if we want that one element is expanded to the adjacent 36 elements instead of 9, we should define 36 information processing units (see Figure 4). This is an example of problem-specific ML that the NN architecture is determined according to the hardware structure.

During the model training, the full CSI is still required to compute the objectives (17a)⁴. However, phase shifts of all RIS elements Φ are computed with the partial CSI after the training in the application, which implies that only the partial CSI on the anchor elements is required in application.

3) *Efficient Parallel Implementation with Tensor Operations:* Although (20) and (21) are the most intuitive way to understand the information flow in RISnet, the computation is done per RIS element (and user), which can only be implemented in a loop and has a low computation efficiency. In order to utilize the parallel computing in a GPU, it would be desirable to implement the information processing as tensor operations instead of computation per RIS element (and user). Let \mathbf{F}_{i+1}^{ca} be the output of information processing unit ca in layer i , the second row of the right hand side of (20) can be rewritten as

$$\mathbf{F}_{i+1}^{ca}[\cdot, n, u] = \left(\sum_{n'} \text{ReLU}(\mathbf{W}_i^{ca} \mathbf{f}_{un', i} + \mathbf{b}_i^{ca}) \right) / N. \quad (23)$$

It is easy to prove that (23) is equivalent to

$$\mathbf{F}_{i+1}^{ca} = \text{ReLU}(\mathbf{W}_i^{ca} \mathbf{F}_i + \mathbf{b}_i^{ca}) \cdot \mathbf{1}^{N \times N} / N, \quad (24)$$

where the multiplication between \mathbf{W}_i^{ca} and \mathbf{F}_i is done in the first dimension (the feature dimension) of \mathbf{F}_i and the multiplication between $\text{ReLU}(\mathbf{W}_i^{ca} \mathbf{F}_i + \mathbf{b}_i^{ca})$ and $\mathbf{1}^{N \times N}$ takes place in the last two dimensions (users and RIS elements) of $\text{ReLU}(\mathbf{W}_i^{ca} \mathbf{F}_i + \mathbf{b}_i^{ca})$. In this way, (23) is computed for all RIS elements and users without a loop using tensor operations. Similarly, the third row of the right hand side of (20) can be rewritten as

$$\mathbf{F}_{i+1}^{oc}[\cdot, n, u] = \left(\sum_{u' \neq u} \text{ReLU}(\mathbf{W}_i^{oc} \mathbf{f}_{u'n, i} + \mathbf{b}_i^{oc}) \right) / (U - 1). \quad (25)$$

It is straightforward to prove that (25) is equivalent to

$$\mathbf{F}_{i+1}^{oc} = \mathbf{E}^{U \times U} \cdot \text{ReLU}(\mathbf{W}_i^{oc} \mathbf{F}_i + \mathbf{b}_i^{oc}) / (U - 1). \quad (26)$$

Other operations in (20)–(21) can also be parallelized in similar ways. Therefore, the RISnet can be implemented in a computation-efficient way.

D. Joint Optimization of BS Precoding and RIS Configuration

Problem (17) involves joint optimization of BS precoding and RIS configuration. Using domain knowledge in communication, we identify WMMSE precoding [5] as a high-performance

⁴The full CSI can be obtained, e.g., by off-line channel measurement before the operation.

analytical precoding scheme. We apply it in order to guarantee precoding performance and reduce training difficulty since we do not need to optimize precoding.

The WMMSE precoding [5] is briefly elaborated as follows: It is first proved that the WSR maximization problem is equivalent to a weighted sum mean squared error (MSE) minimization problem. Following this observation, an iterative algorithm is proposed. In each iteration, the weight of each user's MSE is updated. Subsequently, the precoding matrix for each user is computed. The iteration is terminated if the MSE weights converge. In particular, a factor μ_k (equation (18) in [5]) is computed numerically in the precoding matrix computation in order to meet the transmit power constraint (17b). Therefore, the WMMSE precoder is indifferentiable and cannot be part of the objective because the NN is trained with gradient ascent. As a result, we apply AO, where we fix the NN and compute the precoding matrix \mathbf{V} using the RIS configuration generated by the current RISnet for each data sample in \mathcal{D} , then treat \mathbf{V} as constants and train the NN for the given precoding.

The framework of the hybrid approach of joint optimization is illustrated in Figure 6.

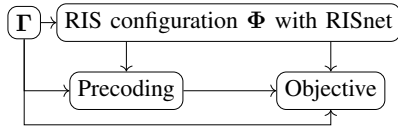


Figure 6. Hybrid solution of analytical precoding and ML-enabled RIS configuration.

The training objective is (17a). Note that although constraints (17b)–(17d) do not appear in the objective, (17b) is fulfilled by the WMMSE algorithm (see equation (18) in [5]), (17c) is satisfied because $|e^{j\varphi}| = 1$ for any $\varphi \in \mathbb{R}$, (17d) is guaranteed because all the off-diagonal elements stay constant throughout training and inference.

Summarizing the above descriptions, the algorithms to train the NN is formulated as Algorithm 1.

Algorithm 1 Neural network training with AO

- 1: Initialize the permutation-invariant RISnet N_θ .
 - 2: **repeat**
 - 3: Randomly choose data samples in a batch.
 - 4: Compute WMMSE precoding matrix according to [5] for every data sample, where the precoding matrix is considered as constants for training.
 - 5: Compute phase shifts Φ with current N_θ .
 - 6: Compute objective (17a) with CSI, user weights, precoding (considered as constants) and phase shifts.
 - 7: Compute gradient of (17a) w.r.t. θ with backward propagation.
 - 8: Perform an optimization with the ADAM optimizer according to the gradient.
 - 9: **until** WSR stops increasing.
-

V. TRAINING AND TESTING RESULTS

The training and testing results are presented in this section. The open-source DeepMIMO data set [38] is applied to generate

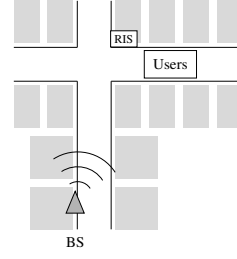


Figure 7. The considered scenario: an intersection in an urban environment.

channel data. The chosen urban scenario is shown in Figure 7, where the LoS channel from BS to users are blocked by a building. Only a weak direct channel is available through reflections on buildings and ground. Furthermore, the channel from BS to RIS has multiple multi-path components (MPCs) such that the MIMO channel matrix has a high rank to support multiple users in SDMA. Finally, we choose users at least 8m from each other to realize a full-rank channel matrix from RIS to users, since the rank of the cascaded channel matrix is less than or equal to the lowest rank of the factors in the product, see Remark 3. The user grouping is assumed given. We note that it is an open topic to assign users according to channel/user positions.

Important assumptions and parameter settings are listed in Table I. It is to note that the performance is sensitive to the learning rate.

Table I
SCENARIO AND MODEL PARAMETERS

Parameter	Value
Number of BS antennas	9
RIS size	36×36 elements
Carrier frequency	3.5 GHz
Distance between adjacent antennas at BS	0.5 wavelength
Distance between adjacent antennas at RIS	0.25 wavelength
Number of users	4
Learning rate	$8 \times 10^{-4} - 1.5 \times 10^{-3}$
Batch size	512
Optimizer	ADAM
Number of data samples in training set	10 240
Number of data samples in testing set	1024

As described in Section IV-C2, the effectiveness of RIS configuration with partial CSI depends on the channel model: the partial CSI contains sufficient information to configure the whole RIS if the channel consist of a few LoS or specular propagation paths. In this case, the channel gains at different RIS elements are strongly correlated spatially because all these channel gains are due to these specular propagation paths. On the contrary, if the channel has infinitely many and infinitely weak propagation paths due to scattering, the channel gains at different RIS elements are spatially independent and identically distributed (i.i.d.) [39]. We assume three channel models to assess the feasibility of applying partial CSI for RIS configuration:

- Deterministic ray-tracing channel from DeepMIMO simulator, which is most feasible to infer the full CSI from the partial CSI.

- Deterministic ray-tracing channel plus i.i.d. scattering gains on each RIS element. It is less feasible to infer the full CSI from the partial CSI with this model.
- I.i.d. channel model due to scattering of infinitely many infinitely weak propagation paths, where the inference of full CSI from partial CSI is impossible.

A. Training Behavior

Figure 8 illustrates the improvement of WSR in training and testing with full and partial CSIs, where the user weights are uniformly randomly generated and sum up to one, and the data for testing is independently generated from the data for training. It can be observed that training and testing with the same setup realize similar performances, suggesting a good generalizability of the trained model. From Figure 8(a), we observe that similar performances are achieved with full and partial CSI when the channel is generated by the ray-tracing simulation and is therefore deterministic, suggesting that the partial CSI is sufficient and the difficulty of channel estimation can be relieved significantly. With the deterministic channel and i.i.d. scattering gain (Figure 8(b)), the realized WSR with partial CSI is lower than with full CSI, because the full CSI cannot be recovered from the partial CSI due to the spatially i.i.d. scattering gain. However, the difference between full and partial CSIs is insignificant, suggesting that the proposed approach is robust against i.i.d. scattering gain. If the channel is spatially fully i.i.d. (Figure 8(c)), the WSR with full CSI is improved significantly, whereas the WSR with partial CSI stays almost constant. This is because we cannot recover full CSI from partial CSI due to the independent channel gains at different RIS elements.

According to [40], the wireless channel is *sparse* in many typical scenarios, i.e., the signal arrives the receiver via a few distinct MPCs and the spatially i.i.d. scattering effect is very limited. This fact is the foundation of many compressed sensing based channel estimation [41], [42]. Since most real wireless channels are similar to deterministic channel model with or without i.i.d. scattering gain (i.e., like Figure 8(a) and Figure 8(b) rather than Figure 8(c)), the proposed method with partial CSI is believed to work well not only in simulation, but also in reality.

B. Comparison with Baselines

Next, we compare our proposed approach with baselines. Since RIS optimization considering mutual coupling for SDMA is still an open topic, we assume an RIS without mutual coupling and use deep reinforcement learning (DRL) [21], random phase shift, and BCD algorithm [6] as baselines for comparison. The problem formulation is with full CSI and without mutual coupling. As a fair comparison with the same problem formulation, we also train RISnet assuming no mutual coupling, i.e., using (1) as the channel model. Figure 9 shows the performance comparison of the proposed approach and the baselines. We have the following observations:

- The proposed RISnet outperforms baseline algorithms DRL, random phase shift and BCD algorithm significantly. The only exception is RISnet with i.i.d. channel gain and

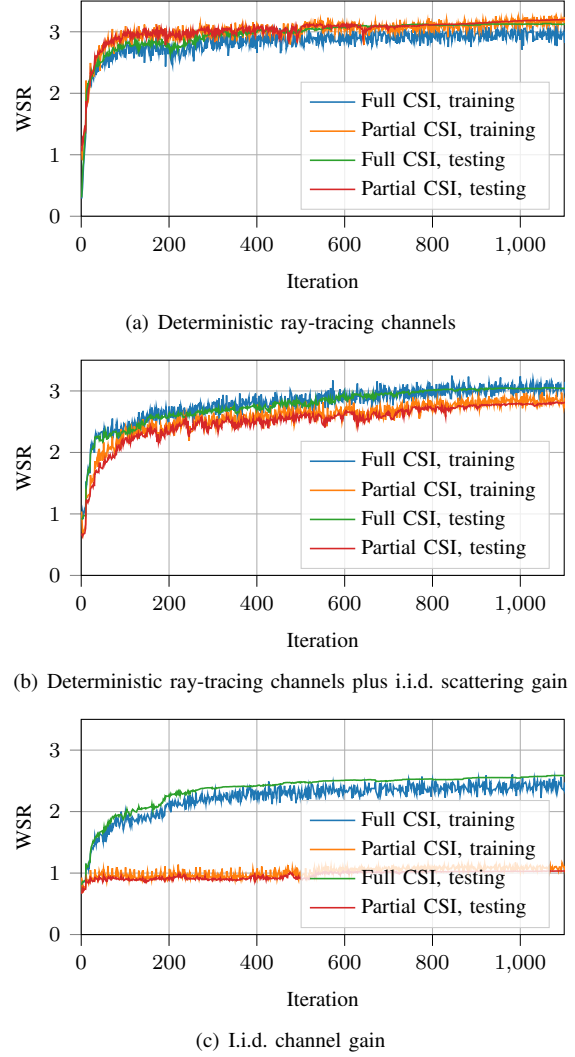


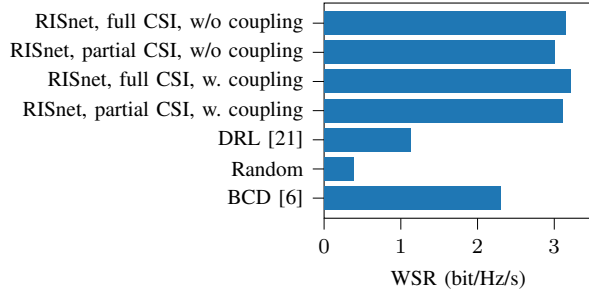
Figure 8. Realized WSR with SDMA in training and testing.

partial CSI, as explained below. A main reason for the better performance of the proposed approach is that DRL with a fully connected NN and BCD algorithm have a poor scalability with the number of RIS elements.

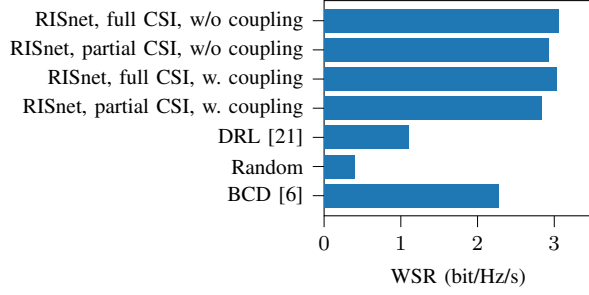
- The proposed RISnet with partial CSI works well with deterministic ray-tracing channel model (Figure 9(a)), and deterministic channel model plus i.i.d. channel gain (Figure 9(b)). The observation holds for both setups with and without mutual coupling. This is because the partial CSI contains sufficient information to recover the full CSI. On the contrary, the full CSI cannot be recovered from the partial CSI with i.i.d. channel gain. Therefore, the performance with partial CSI and i.i.d. channel gain is poor.

C. Necessity to Consider Mutual Coupling

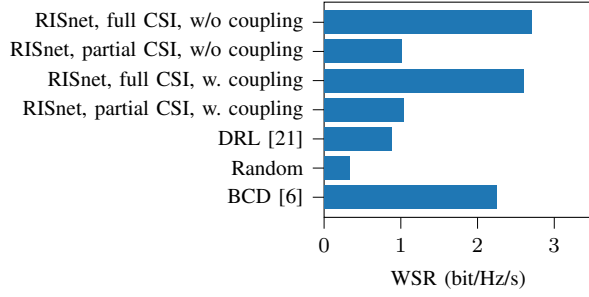
In this section, we demonstrate the necessity to consider mutual coupling by testing RISnet trained *without mutual coupling* to problem *with mutual coupling*. As shown in Figure 10, the model mismatch (i.e., model trained without mutual coupling and tested with mutual coupling) results in



(a) Deterministic ray-tracing channels



(b) Deterministic ray-tracing channels plus i.i.d. scattering gain



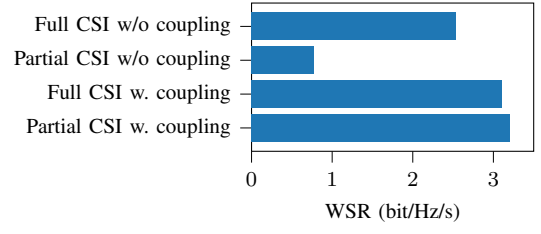
(c) I.i.d. channel gain

Figure 9. Comparison between proposed approach with baselines. The proposed approach outperforms all baselines with the exception of partial CSI and i.i.d. channel gain.

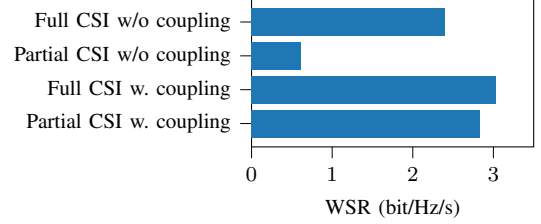
a significant degradation particularly for RISnet with partial CSI, which justifies the necessity of explicit consideration of mutual coupling if it exists in the RIS hardware.

D. Performance with Different Numbers of Anchor Elements

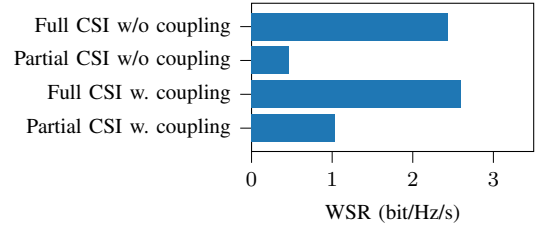
In this section, we investigate the impact of the anchor element number on the performance. We consider a RIS with 16 anchor elements with the ability of channel estimation, as depicted in Figure 4, and a RIS with 4 anchor elements. We expect that the RIS with 4 anchor elements is more vulnerable to i.i.d. scattering gain due to the less input information. The realized WSR is shown in Figure 11. The two RISs are roughly equally good with deterministic channels and roughly equally bad with i.i.d. channel gain. However, the RIS with 16 anchor elements (more partial CSI) performs much better than the RIS with 4 anchor elements (less partial CSI), as we expect. This result suggests that the required number of anchor elements depends on the channel property: The more i.i.d. scattering gain, the more required anchor elements and more expensive



(a) Deterministic ray-tracing channels



(b) Deterministic ray-tracing channels plus i.i.d. scattering gain



(c) I.i.d. channel gain

Figure 10. Comparison between testing results considering mutual coupling of trained models without (first two rows) and with (last two rows) consideration of mutual coupling. This result justifies the necessity to consider mutual coupling if it exists because the model mismatch results in significant performance loss.

hardware. The optimal choice of the hardware depends on the propagation environment.

E. Complexity Analysis

In addition to performance, another major advantage of RISnet is the low complexity in real-time application. According to (24) and (26), the information processing of a layer is considered as cascading operation of tensor multiplication and addition of complexity $\mathcal{O}(QPKN) + \mathcal{O}(QKN)$, where P is the input feature dimension and Q is the output feature dimension, the ReLU activation of complexity $\mathcal{O}(QKN)$ (because the activation function is performed element-wise), and the averaging operation of complexity $\mathcal{O}(N)$, $\mathcal{O}(U)$ and $\mathcal{O}(NU)$ for class ca, oc and oa, respectively. Asymptotically, the complexity of RISnet inference is $\mathcal{O}(QPKN)$. On the other hand, the asymptotical complexity of the BCD algorithm is $\mathcal{O}(U^2N^2)$ [6]. The asymptotical complexity of a fully connected NN applied in [21] is $\mathcal{O}(UN^2)$ since the input dimension is proportional to UN (number of users times number of RIS elements) and the output dimension is N . We can see clearly that the complexity of RISnet inference grows linearly with the number of RIS elements N , while the complexities of baseline approaches [6], [21] grow quadratically with N . This observation confirms the high scalability of the proposed RISnet.

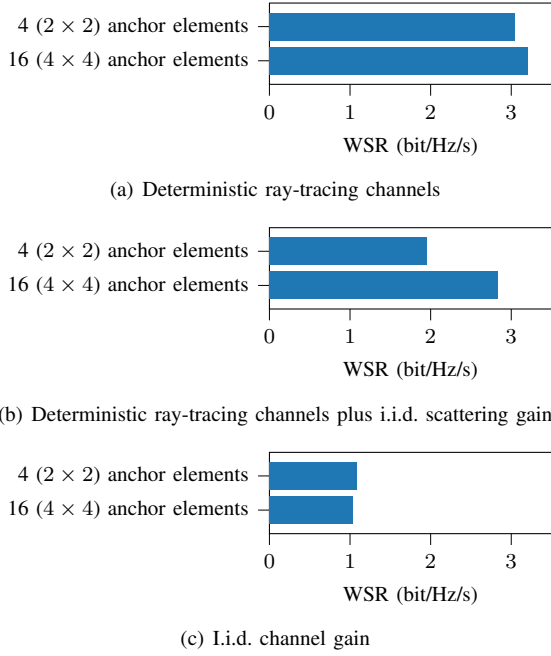


Figure 11. Comparison between training results with different numbers of anchor elements. More anchor elements have higher hardware complexity but are more robust to i.i.d. channel gain.

Practically, RISnet can configure a RIS with 1296 elements within 0.07 second on an off-the-shelf laptop with Apple M3 Pro processor, while reference [6] needs 253 seconds and reference [21] needs 0.23-second. The reason of the fast inference is that the most computation complexity is in training, which takes about 8 hours. Once the training is finished, the inference (application) with a trained RISnet is very efficient. Compared to a fully connected NN, where the number of trainable parameters is proportional to the product of input and output dimensions, the number of trainable parameters of RISnet is independent from the input and output dimensions. This comparison shows the advantage of complexity and real-time performance of the proposed RISnet. In future applications, we can leverage the hardware developed for heavy ML applications such as large language models (LLMs) and autonomous driving in a much smaller scale, because the proposed RISnet has about 10^4 trainable parameters, which is one million times less than current LLMs [43], making an efficient real-time application feasible with low-cost hardware.

VI. CONCLUSION

The SDMA technique is crucial in multi-user wireless communication system. Its performance depends strongly on the channel property, which can be improved by the RIS. In the previous research, scalability of RIS elements, unrealistic assumption of full CSI and ignorance of mutual coupling between adjacent RIS elements are the main limitations of realizing RIS in reality. In this work, we have focused on deriving scalable solutions with unsupervised ML for RIS configuration while making realistic assumptions regarding CSI knowledge and mutual coupling between adjacent RIS elements. We integrate domain-knowledge in communication and ML

techniques to design a problem-specific NN architecture *RISnet*, which is permutation-invariant to user input. We further showed that partial CSI is sufficient to achieve a similar performance to full CSI if the channel comprises of a few specular propagation paths (i.e., the channel gain is not dominated by i.i.d. components due to scattering). Finally, we demonstrated that the proposed approach outperforms the baselines significantly and it is necessary to explicitly consider the mutual coupling. Beyond this work, problem-specific ML combining domain knowledge and ML techniques provides unique opportunity to improve performance, complexity and equivariance compared to generic ML. This work can be extended by considering rate-splitting multiple access (RSMA) and beyond-diagonal RIS.

Code and data in this paper are available under https://github.com/bilepeng/risnet_mutual_partial.

APPENDIX A PROOF OF THEOREM 1

We first prove that every layer except the last layer is permutation-equivariant, i.e., if $\mathbf{F}'_i = \mathbf{P} \cdot \mathbf{F}_i$, where \mathbf{P} is an arbitrary permutation matrix and the multiplication is between \mathbf{P} and the last two dimensions of \mathbf{F}_i , $\mathbf{F}_{i+1} = M(\mathbf{F}_i)$ and $\mathbf{F}'_{i+1} = M(\mathbf{F}'_i)$, where M is a layer, we have $\mathbf{F}'_{i+1} = \mathbf{P} \cdot \mathbf{F}_{i+1}$.

We first consider class cc, the output of information processing unit cc of layer i given the permuted input is

$$\mathbf{F}'_{i+1}{}^{\text{cc}} = \text{ReLU}(\mathbf{W}_i^{\text{cc}} \mathbf{P} \cdot \mathbf{F}_i + \mathbf{b}_i^{\text{cc}}) \quad (27)$$

$$= \text{ReLU}(\mathbf{P} \cdot \mathbf{W}_i^{\text{cc}} \mathbf{F}_i + \mathbf{b}_i^{\text{cc}}) \quad (28)$$

$$= \mathbf{P} \cdot \text{ReLU}(\mathbf{W}_i^{\text{cc}} \mathbf{F}_i + \mathbf{b}_i^{\text{cc}}) \quad (29)$$

$$= \mathbf{P} \mathbf{F}_{i+1}{}^{\text{cc}}. \quad (30)$$

The second line holds because the multiplication with \mathbf{W}_i^{cc} is in the first dimension of $\mathbf{P} \cdot \mathbf{F}_i$, whereas the multiplication with \mathbf{P} is in the second and the third dimensions of \mathbf{F}_i . The third line holds because ReLU is an elementwise operation. The fourth line is the definition of $\mathbf{F}_{i+1}^{\text{cc}}$. Similarly, we can prove $\mathbf{F}'_{i+1}{}^{\text{ca}} = \mathbf{P} \cdot \mathbf{F}_{i+1}{}^{\text{ca}}$.

To prove $\mathbf{F}'_{i+1}{}^{\text{oc}} = \mathbf{P} \cdot \mathbf{F}_{i+1}{}^{\text{oc}}$, we first need to prove the multiplication between $\mathbf{E}^{U \times U}$ and \mathbf{P} is commutative:

$$\mathbf{E}^{U \times U} \mathbf{P} = \mathbf{1}^{U \times U} \mathbf{P} - \mathbf{I}^{U \times U} \mathbf{P} \quad (31)$$

$$= \mathbf{P} \mathbf{1}^{U \times U} - \mathbf{P} \mathbf{I}^{U \times U} \quad (32)$$

$$= \mathbf{P} \mathbf{E}^{U \times U}. \quad (33)$$

The third line holds because the sum of every row/column of \mathbf{P} is 1. We can now prove the permutation-equivariance as

$$\begin{aligned} \mathbf{F}'_{i+1}{}^{\text{oc}} &= \mathbf{E}^{U \times U} \cdot \text{ReLU}(\mathbf{W}_i^{\text{oc}} \mathbf{P} \cdot \mathbf{F}_i + \mathbf{b}_i^{\text{oc}}) / (U - 1) \\ &= \mathbf{E}^{U \times U} \cdot \text{ReLU}(\mathbf{P} \cdot \mathbf{W}_i^{\text{oc}} \mathbf{F}_i + \mathbf{b}_i^{\text{oc}}) / (U - 1) \\ &= \mathbf{E}^{U \times U} \mathbf{P} \cdot \text{ReLU}(\mathbf{W}_i^{\text{oc}} \mathbf{F}_i + \mathbf{b}_i^{\text{oc}}) / (U - 1) \\ &= \mathbf{P} \cdot \mathbf{E}^{U \times U} \text{ReLU}(\mathbf{W}_i^{\text{oc}} \mathbf{F}_i + \mathbf{b}_i^{\text{oc}}) / (U - 1) \\ &= \mathbf{P} \cdot \mathbf{F}_{i+1}{}^{\text{oc}}. \end{aligned}$$

Similarly, we can prove $\mathbf{F}'_{i+1}{}^{\text{oa}} = \mathbf{P} \cdot \mathbf{F}_{i+1}{}^{\text{oa}}$.

Since the output of every class in every layer is permutation-equivariant, the whole output after summation over users is permutation-invariant.

REFERENCES

- [1] B. Peng, K.-L. Besser, R. Raghunath, V. Jamali, and E. A. Jorswieck, "RISnet: A scalable approach for reconfigurable intelligent surface optimization with partial CSI," in *2023 IEEE Glob. Commun. Conf. (GLOBECOM)*, IEEE, Dec. 2023.
- [2] C.-Y. Wei, J. Akhtman, S. X. Ng, and L. Hanzo, "Iterative near-maximum-likelihood detection in rank-deficient downlink SDMA systems," *IEEE Trans. Veh. Technol.*, vol. 57, no. 1, pp. 653–657, 2008.
- [3] Y. Liu, X. Liu, X. Mu, T. Hou, J. Xu, M. Di Renzo, and N. Al-Dhahir, "Reconfigurable intelligent surfaces: Principles and opportunities," *IEEE Commun. Surv. & Tutor.*, vol. 23, no. 3, pp. 1546–1577, 2021.
- [4] M. Joham, W. Utschick, and J. A. Nossek, "Linear transmit processing in MIMO communications systems," *IEEE Trans. Signal Process.*, vol. 53, no. 8, pp. 2700–2712, 2005.
- [5] Q. Shi, M. Razaviyayn, Z.-Q. Luo, and C. He, "An iteratively weighted MMSE approach to distributed sum-utility maximization for a MIMO interfering broadcast channel," *IEEE Trans. Signal Process.*, vol. 59, no. 9, pp. 4331–4340, 2011.
- [6] H. Guo, Y.-C. Liang, J. Chen, and E. G. Larsson, "Weighted sum-rate maximization for reconfigurable intelligent surface aided wireless networks," *IEEE Trans. Wirel. Commun.*, vol. 19, no. 5, pp. 3064–3076, 2020.
- [7] C. Huang, A. Zappone, M. Debbah, and C. Yuen, "Achievable rate maximization by passive intelligent mirrors," in *2018 IEEE Int. Conf. Acoust. Speech Signal Process. (ICASSP)*, IEEE, 2018, pp. 3714–3718.
- [8] G. Zhou, C. Pan, H. Ren, K. Wang, and A. Nallanathan, "Intelligent reflecting surface aided multigroup multicast MISO communication systems," *IEEE Trans. Signal Process.*, vol. 68, pp. 3236–3251, 2020.
- [9] X. Liu, C. Sun, and E. A. Jorswieck, "Two-user SINR region for reconfigurable intelligent surface aided downlink channel," in *2021 IEEE Int. Conf. Commun. Work. (ICC Work.)*, IEEE, 2021, pp. 1–6.
- [10] Z. Li, M. Hua, Q. Wang, and Q. Song, "Weighted sum-rate maximization for multi-IRS aided cooperative transmission," *IEEE Wirel. Commun. Lett.*, vol. 9, no. 10, pp. 1620–1624, 2020.
- [11] Q. Wu and R. Zhang, "Beamforming optimization for wireless network aided by intelligent reflecting surface with discrete phase shifts," *IEEE Trans. Commun.*, vol. 68, no. 3, pp. 1838–1851, 2019.
- [12] R. Long, Y.-C. Liang, Y. Pei, and E. G. Larsson, "Active reconfigurable intelligent surface-aided wireless communications," *IEEE Trans. Wirel. Commun.*, vol. 20, no. 8, pp. 4962–4975, 2021.
- [13] M. A. Elmassallamy, H. Zhang, R. Sultan, K. G. Seddik, L. Song, Z. Han, and Z. Han, "On spatial multiplexing using reconfigurable intelligent surfaces," *IEEE Wirel. Commun. Lett.*, vol. 10, no. 2, pp. 226–230, 2021.
- [14] Z. Lin, H. Niu, K. An, Y. Wang, G. Zheng, S. Chatzinotas, and Y. Hu, "Refracting RIS-aided hybrid satellite-terrestrial relay networks: Joint beamforming design and optimization," *IEEE Trans. Aerosp. Electron. Syst.*, vol. 58, no. 4, pp. 3717–3724, Aug. 2022.
- [15] K. An, Y. Sun, Z. Lin, Y. Zhu, W. Ni, N. Al-Dhahir, K.-K. Wong, and D. Niyato, "Exploiting multi-layer refracting RIS-assisted receiver for HAP-SWIPT networks," *IEEE Trans. Wirel. Commun.*, vol. 23, no. 10, pp. 12 638–12 657, Oct. 2024.
- [16] M. Di Renzo, A. Zappone, M. Debbah, M.-S. Alouini, C. Yuen, J. De Rosny, and S. Tretakov, "Smart radio environments empowered by reconfigurable intelligent surfaces: How it works, state of research, and the road ahead," *IEEE J. Sel. Areas Commun.*, vol. 38, no. 11, pp. 2450–2525, 2020.
- [17] M. Najafi, V. Jamali, R. Schober, and H. V. Poor, "Physics-based modeling and scalable optimization of large intelligent reflecting surfaces," *IEEE Trans. Commun.*, vol. 69, no. 4, pp. 2673–2691, 2020.
- [18] K. Hornik, M. Stinchcombe, and H. White, "Multilayer feedforward networks are universal approximators," *Neural Netw.*, vol. 2, no. 5, pp. 359–366, 1989.
- [19] R. Zhong, Y. Liu, X. Mu, Y. Chen, and L. Song, "AI empowered RIS-assisted NOMA networks: Deep learning or reinforcement learning?" *IEEE J. Sel. Areas Commun.*, vol. 40, no. 1, pp. 182–196, 2021.
- [20] X. Gao, Y. Liu, X. Liu, and L. Song, "Machine learning empowered resource allocation in IRS aided MISO-NOMA networks," *IEEE Trans. Wirel. Commun.*, vol. 21, no. 5, pp. 3478–3492, 2021.
- [21] C. Huang, R. Mo, and C. Yuen, "Reconfigurable intelligent surface assisted multiuser MISO systems exploiting deep reinforcement learning," *IEEE J. Sel. Areas Commun.*, vol. 38, no. 8, pp. 1839–1850, 2020.
- [22] M. Shehab, B. S. Ciftler, T. Khattab, M. M. Abdallah, and D. Trinchero, "Deep reinforcement learning powered IRS-assisted downlink NOMA," *IEEE Open J. Commun. Soc.*, vol. 3, pp. 729–739, 2022.
- [23] Y. Guo, F. Fang, D. Cai, and Z. Ding, "Energy-efficient design for a NOMA assisted STAR-RIS network with deep reinforcement learning," *IEEE Trans. Veh. Technol.*, vol. 72, no. 4, pp. 5424–5428, Apr. 2022.
- [24] B. Sheen, J. Yang, X. Feng, and M. M. U. Chowdhury, "A deep learning based modeling of reconfigurable intelligent surface assisted wireless communications for phase shift configuration," *IEEE Open J. Commun. Soc.*, vol. 2, pp. 262–272, 2021.
- [25] T. Jiang, H. V. Cheng, and W. Yu, "Learning to reflect and to beamform for intelligent reflecting surface with implicit channel estimation," *IEEE J. Sel. Areas Commun.*, vol. 39, no. 7, pp. 1931–1945, 2021.
- [26] Ö. Özdoğan and E. Björnson, "Deep learning-based phase reconfiguration for intelligent reflecting surfaces," in *2020 54th Asilomar Conf. Signals Syst. Comput.*, IEEE, 2020, pp. 707–711.
- [27] G. Yang, X. Xu, Y.-C. Liang, and M. Di Renzo, "Reconfigurable intelligent surface-assisted non-orthogonal multiple access," *IEEE Trans. Wirel. Commun.*, vol. 20, no. 5, pp. 3137–3151, 2021.
- [28] J. An, C. Xu, Q. Wu, D. W. K. Ng, M. Di Renzo, C. Yuen, and L. Hanzo, "Codebook-based solutions for reconfigurable intelligent surfaces and their open challenges," *IEEE Wirel. Commun.*, 2022.
- [29] X. Qian and M. Di Renzo, "Mutual coupling and unit cell aware optimization for reconfigurable intelligent surfaces," *IEEE Wirel. Commun. Lett.*, vol. 10, no. 6, pp. 1183–1187, 2021.
- [30] G. Gradoni and M. Di Renzo, "End-to-end mutual coupling aware communication model for reconfigurable intelligent surfaces: An electromagnetic-compliant approach based on mutual impedances," *IEEE Wirel. Commun. Lett.*, vol. 10, no. 5, pp. 938–942, 2021.
- [31] G. Pettanice, R. Valentini, P. Di Marco, F. Loreto, D. Romano, F. Santucci, D. Spina, and G. Antonini, "Mutual coupling aware time-domain characterization and performance analysis of reconfigurable intelligent surfaces," *IEEE Trans. Electromagn. Compat.*, 2023.
- [32] S. Shen, B. Clerckx, and R. Murch, "Modeling and architecture design of reconfigurable intelligent surfaces using scattering parameter network analysis," *IEEE Trans. Wirel. Commun.*, vol. 21, no. 2, pp. 1229–1243, 2021.
- [33] M. Nerini, S. Shen, H. Li, M. Di Renzo, and B. Clerckx, *A universal framework for multiport network analysis of reconfigurable intelligent surfaces*, Nov. 2023. arXiv: 2311.10561 [cs.IT].
- [34] T. Dash, S. Chitlangia, A. Ahuja, and A. Srinivasan, "A review of some techniques for inclusion of domain-knowledge into deep neural networks," *Sci. Rep.*, vol. 12, no. 1, 1040, 2022.
- [35] Y. Mao, O. Dizdar, B. Clerckx, R. Schober, P. Popovski, and H. V. Poor, "Rate-splitting multiple access: Fundamentals, survey, and future research trends," *IEEE Commun. Surv. & Tutor.*, vol. 24, no. 4, pp. 2073–2126, 2022.
- [36] W. Yu, F. Söhrabi, and T. Jiang, "Role of deep learning in wireless communications," *IEEE BITS Inf. Theory Mag.*, vol. 2, no. 2, pp. 56–72, Nov. 2022.
- [37] Y. Ju, S. Gong, H. Liu, C. Xing, J. An, and Y. Li, "Beamforming optimization for hybrid active-passive RIS assisted wireless communications: A rate-maximization perspective," *IEEE Trans. Commun.*, 2024.
- [38] A. Alkhateeb, "DeepMIMO: A generic deep learning dataset for millimeter wave and massive MIMO applications," in *Proc. Inf. Theory Appl. Work. (ITA)*, San Diego, CA, Feb. 2019.
- [39] V. Jamali, W. Ghanem, R. Schober, and H. V. Poor, "Impact of channel models on performance characterization of RIS-assisted wireless systems," in *Eur. Conf. Antennas Propag. (EuCAP)*, 2023.
- [40] R. He, B. Ai, G. Wang, M. Yang, C. Huang, and Z. Zhong, "Wireless channel sparsity: Measurement, analysis, and exploitation in estimation," *IEEE Wirel. Commun.*, vol. 28, no. 4, pp. 113–119, 2021.
- [41] S. Haghighatshoar and G. Caire, "Massive MIMO pilot decontamination and channel interpolation via wideband sparse channel estimation," *IEEE Trans. Wirel. Commun.*, vol. 16, no. 12, pp. 8316–8332, 2017.
- [42] G. Wunder, S. Stefanatos, A. Flinthe, I. Roth, and G. Caire, "Low-overhead hierarchically-sparse channel estimation for multiuser wideband massive MIMO," *IEEE Trans. Wirel. Commun.*, vol. 18, no. 4, pp. 2186–2199, 2019.
- [43] W. X. Zhao, K. Zhou, J. Li, T. Tang, X. Wang, Y. Hou, Y. Min, B. Zhang, J. Zhang, Z. Dong, et al., *A survey of large language models*, Mar. 2023. arXiv: 2303.18223 [cs.CL].